Available online at www.sciencedirect.com

SciVerse ScienceDirect

Journal of the European Ceramic Society 32 (2012) 2043–2051

www.elsevier.com/locate/jeurceramsoc

Nanoindentation, AFM and tribological properties of thin nc-WC/a-C Coatings

František Lofaj [a,b,*], Milan Ferdinandy [a], Gregorz Cempura [c], Ján Dusza [a,b]

[a] Institute of Materials Research of SAS, Watsonova 47, 040 01 Košice, Slovakia

[b] Faculty of Materials Science and Technology in Trnava, Slovak University of Technology in Bratislava, Paulínska 16, 916 24 Trnava, Slovakia

[c] Faculty of Metals Engineering and Industrial Computer Science, AGH University of Science and Technology, Al. A. Mickiewicza 30, PL-30059 Kraków, Poland

Available online 12 March 2012

Abstract

Instrumented indentation, AFM (atomic force microscopy) and tribological studies were performed on PE CVD (Plasma Enhanced Chemical Vapor Deposition) nanocomposite WC–C coatings to investigate the effects of surface roughness on the reliability of nanoindentation data and the possibilities of different AFM modes in nanomechanical testing, which can be used as a feedback to optimize deposition technology from the viewpoint of their mechanical properties. It was confirmed that surface roughness below 30 nm is necessary to keep the scatter of indentation modulus, E_{IT}, and hardness, H_{IT}, below 15%. PF QNM (Peak Force Quantitative NanoMechanical) mode was successfully applied for qualitative mapping of the elastic modulus of coatings with the stiffness above 300 GPa. LFM (lateral force microscopy) mode showed only weak contrast and quantitative measurements in both AFM modes require precise calibration. Coefficients of friction of the studied WC–C coatings were below 0.2 at RT, but increased to 0.7–0.8 at 450 °C due to the formation of a transfer film. Optimization of the deposition conditions based on nanoindentation resulted in the increase of E_{IT} from ~220 GPa to 350 GPa and H_{IT} from ~17 GPa to ~29 GPa.

Keywords: A. Films; B. Nanocomposites; C. Hardness; C. Wear resistance; Elastic modulus mapping

1. Introduction

The increase of the effectiveness of the cutting operations during metal machining is possible either by using for cutting inserts materials with better mechanical properties or by application of thin coatings, which provide sufficient increase in mechanical properties of the whole insert. When coatings are used, their hardness is among the critical parameters affecting the performance of cutting tools. Harder coatings enable higher cutting speeds, so there is a tendency to produce coatings as hard as possible. The principal ways leading to higher hardness include using intrinsically harder materials for the coatings, introduction of high compressive stresses and/or nanocomposite coatings. In the last case, nanocomposite coatings exhibit substantial hardness increase compared to the same coatings with conventional structure due to size of grains embedded in the amorphous matrix so small, that dislocations cannot exist inside the individual crystallites. The principles for obtaining the superhard (15–40 GPa) and ultrahard (>40 GPa) coatings were suggested by Veprek for nanoparticles of TiC in the amorphous silicon nitride matrix coatings.[1] However, the approach can be applied to many other systems. Diamond-like carbon coatings as a part of amorphous (hydrogenated) carbon (a-C:H) coatings exhibit high intrinsic hardness, low coefficients of friction (COF) and high wear resistance. Introduction of nanocrystalline MeC or MeN_xC (Me = W, Ti, Cr, Zr, etc.) phase into amorphous carbon matrix based on Veprek's concept results in the additional increase of hardness, adhesion, toughness and wear resistance of such composites while still retaining low friction coefficients.[1–5] The properties are, obviously, controlled by the amorphous matrix, nanocrystalline phase as well as by the ratio between the content of nanocrystalline carbide phase and carbon-based matrix. The increase of the content of graphitic carbon at the expense of MeC is expected to negatively reduce hardness on one side, but positively increase COF on the other side.

Hydrogenated WC/a-C:H coatings are usually prepared by reactive magnetron sputtering of W or WC in Ar-hydrocarbon plasma. The studies on non-hydrogenated nanocomposite WC/a-C coatings prepared by plasma enhanced CVD methods

* Corresponding author at: Institute of Materials Research of SAS, Watsonova 47, 040 01 Košice, Slovakia. Tel.: +421 55 7922461.
E-mail address: flofaj@imr.saske.sk (F. Lofaj).

0955-2219/$ – see front matter © 2012 Elsevier Ltd. All rights reserved.
doi:10.1016/j.jeurceramsoc.2012.01.037

(PE CVD) are considerably less frequent. Some aspects of their mechanical properties were studied by Yang, Liu, Zeng, and others.[3,4,6–8] Instrumented indentation technique used for the measurement of hardness and elastic properties yielded hardness variations from 5 GPa up to superhardness with typical values of around 15–20 GPa. Elastic modulus of such coatings covered wide range from 120 GPa up to 400 GPa.[8] The scatter results not only from coating structure variations but also from the influence of substrate. The requirements of standard practice for correct measurement on thin films from ISO 14577 – Part 4 are[9]:

- the total penetration depth, h, is less than half of the coating thickness;
- no cracking occurs;
- hardness of the coating is evaluated as a maximum or the plateau that appears in the hardness – penetration depth curve;
- surface roughness, $R_a < 5\%\ h_c$ (h_c is the penetration depth);
- h_c must be smaller than 10–15% of the film thickness to prevent substrate influence.

The requirements can be satisfied when the indentation loads are reduced to μN or even nN range depending on the thickness and stiffness of the studied coatings. New indentation modes were also developed. So-called "continuous multi-cycle" (CMC) mode with several partial unloadings during continuous loading to the maximum load provides information for the determination of hardness/indentation modulus – penetration depth curve required by the ISO standard. Sinusoidal loading mode is the CMC variation when small, but relatively high frequency load oscillations are applied over the main loading. This method gives not just hardness and indentation modulus evolution, but also storage modulus and other parameters as a function of penetration depth. The absolute values obtained from indentation methods are influenced by the indentation size effect (ISE),[11–13] effects of residual stresses,[14,15] surface roughness,[16,17], etc.,[10] which result in an excessive data scatter. Similar arguments are valid also for the measurement of friction and wear properties of the coatings (residual stresses and surface roughness increase their influence on friction under lower loads). The effect of surface roughness on friction and hardness can be partially eliminated when these properties are measured at nano-scale, e.g., by atomic force microscopy (AFM).

The first AFM capable measuring friction forces and thus model the forces in single asperity contact was developed by Mate et al. in 1987.[18] Further development based on the measurement of torsional deflection of the cantilever during lateral motion of a tip on the sample surface and its detection by means of reflected laser beam by 4-segmented photodiod[19,20] led to commercial "friction force microscopy" (FFM) and/or lateral force microscopy (LFM). These techniques enable simultaneous measurements of surface topography and friction forces, so that the effect of surface roughness can be eliminated. However, adhesion forces and other problems related to precise calibration make quantitative measurements of COF even with these microscopes rather difficult.[21]

Besides friction force visualization in AFM at nano-scale level, other modes such as "Force Modulation Microscopy" (FMM) and "Peak Force Tapping" (PFT) can be used for mapping of the elastic properties. FMM uses contact mode imaging superimposed with a sinusoidal cantilever or sample oscillation small enough to keep the tip in contact with the sample. It enables qualitative visualization of differences in mechanical properties from amplitude and phase shift of the cantilever movement compared to the driving oscillation. PFT uses direct fast force distance curve acquisition by a large sinusoidal z-piezo modulation, periodically contacting and separating the tip and the sample. The z-movement is synchronized with lateral sample scanning to ensure controlled maximum impact force down to pN-level, which is used as the imaging setpoint. Additional treatment of the realtime force–distance curves obtained during each cycle included in the so-called "Peak Force Quantitative NanoMechanical" (PF QNM) mode delivers simultaneously to the topographic height a signal proportional to the elastic modulus. It enables (when properly calibrated) even quantitative measurements of elastic properties at a nanoscale level.[22] However, PF QNM has been so far successfully applied only on materials with stiffness below 70 GPa, e.g., biological tissues and polymers.

The aims of this work include investigations of selected mechanical properties (elastic modulus, hardness and friction behavior) of thin PECVD nc-WC/a-C coatings at nanolevel by means of AFM, instrumented nanoindentation and at macrolevel by conventional tribological testing. Special focus is put on the determination of the influence of surface roughness on the uncertainty of nanoindentation data and possibilities of different AFM modes in nanomechanical testing, which can be used as a feedback to optimize PECVD technology from the viewpoint of their mechanical properties. Although the work is a part of larger investigation oriented toward optimization of PE CVD WC–C coatings, it is intentionally limited only to the nanoindentation and tribological behavior of the optimized coatings.

2. Experimental procedure

The studied nc-WC/a-C coatings were deposited on the set of around 25 substrates with the diameter of 55 mm and thickness of ~3 mm made from tempered and annealed tool steel (STN 412050). At first, all substrate surfaces were ground flat with a diamond wheel. Two substrates were left as-ground and the remaining were polished using 15 μm, 6 μm, 3 μm, and 1 μm diamond slurries. One of the well-polished substrates was subsequently wet ground on #80 SiC paper, two on the 80/63 diamond disc and another two substrates on a polishing cloth with 15 μm diamond slurry to obtain substrates with different levels of surface roughness. The rest of the substrates remained as-polished. Surface roughness of all substrates was characterized using contact profilometer (model SJ 201, Mitotuyo) and parameters including arithmetic average of absolute values, R_a, average distance between the highest peak and lowest valley, R_z, and root mean square, R_q, from ten measurements. They were measured along ten lines 10 mm long and 1 mm apart. The same parameters and surface skewness, R_{sk}, were measured at micro-scale on two 50 μm × 50 μm images using AFM (model Dimension Icon, Bruker Co., USA). They were automatically

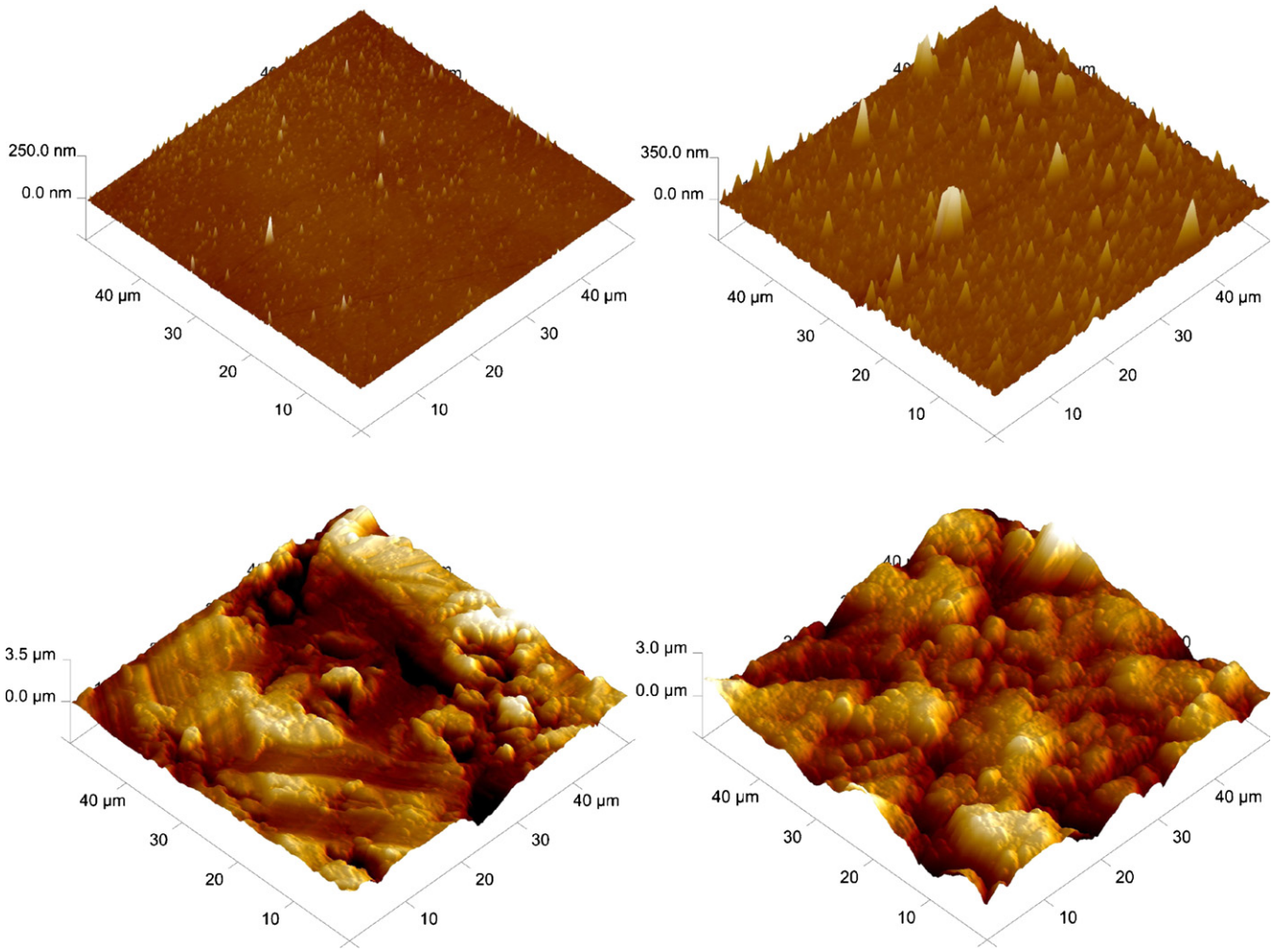

Fig. 1. AFM images of (a) steel substrates after polishing by 1 μm diamond slurry, (b) of the WC–C coating on the substrate after 1 μm polishing (spikes on the image are the artifacts); (c) steel substrate after wet griding using 80/63 μm diamond disc, and (d) topography of WC–C coating deposited on the substrate after 80/63 μm grinding.

calculated for ten 10 μm × 10 μm areas arbitrarily distributed on both images and then averaged.

PECVD WC/C coating with the thickness of around 500 nm has been simultaneously deposited on the set of 7 substrates with controlled roughness. The deposition conditions were: total pressure 3 Pa, current density 1 mA/cm^2 and bias voltage −5 kV. The remaining 18 substrates were coated under different conditions used to maximize nanohardness and minimize coefficient of friction. The main parameter changed during the optimization process was total pressure while the current density and bias, which were optimized during the earlier stage, were kept constant. The details of the optimization process are described in our earlier works,[23,24] exceed the scope of the paper. Surface roughness of the coatings was determined in the same way as in the case of substrates.

Static and dynamic lateral force microscopy was used to visualize friction forces on the coating surfaces. Coefficients of frictions (COF) were not determined due to absence of calibration. However, COF of the coatings were directly measured as a function of sliding distance at different sliding rates and at room temperature, 100 °C and 450 °C in air and in flowing N_2 using high temperature tribometer (model HTT, CSM, Switzerland) with the ball-on-disc method. The constant load of 0.5 N and four sliding rates – 5 cm/s, 10 cm/s, 15 cm/s and 30 cm/s were used in the study. The counterface of the coatings was a 100Cr6 steel ball with the diameter of 6 mm. A new ball was used for each test. The wear areas on the balls were observed by scanning electron microscopy (SEM) combined with energy dispersive X-ray spectroscopy (EDX).

Instrumented hardness and indentation modulus of WC–C coatings were measured with instrumented indentation apparatus (model NHT, CSM, Switzerland) and Berkovich indenter using continuous stiffness measurement (CSM) method and sinusoidal loading (10 Hz) up to 10 mN load from at least 20 indents. The values of indentation hardness and modulus of the coatings were determined according to the ISO standard from the peak in the corresponding depth profiles.

Additional visualization of the elastic modulus distribution in the coatings was made in PF QNM mode using custom-made cantilever with extremely high spring constant (2000 N/m) and

diamond tip as an AFM probe. Peak forces were held constant in the low μN-range during acquisition of simultaneous topographical and mechanical data.

3. Results

3.1. Surface topography

AFM images in Fig. 1 illustrate the topography of the steel substrates after polishing with 1 μm diamond slurry and 80/60 diamond disc and the corresponding WC–Co coatings. The images were used to evaluate surface characteristics by AFM. The results of both contact profilometry and AFM are summarized in Table 1. They include averaged values of surface roughness, R_a, averaged distance between the highest peak and lowest valley, R_z, average root mean square, R_q, and in case of AFM also average skewness, R_{sk}. Subsequent comparison of property dependencies on these parameters revealed that R_a produces the most consistent behavior. Thus, only R_a dependencies were further considered. R_a range on the substrates is 24–570 nm and 3–304 nm, respectively. The corresponding values in the coatings were 100–623 nm and 16–180 nm. Other parameters sometimes exhibit significant variations. Note that values of surface roughness parameters from profilometery are usually higher than from AFM. This is because the contact profilometry values were obtained from the areas of around 100 mm^2 whereas AFM data are obtained from the area of only 1000 μm^2. In later cases, only the zones without artifacts and anomalies were selected.

3.2. Hardness and elastic modulus

Depth profiles of indentation modulus of the studied WC/C coatings were obtained using continuous stiffness measurement method during instrumented indentation (Fig. 2). The dependence of the elastic modulus on penetration depth exhibits a peak at around 50 nm. This depth corresponds to approximately 10% of the coating thickness and satisfies the ISO 14577-4 requirement. The indentation modulus of the coating at the peak position, which corresponds to the coating properties without the influence of the substrate, is approximately 235 ± 29 GPa. The

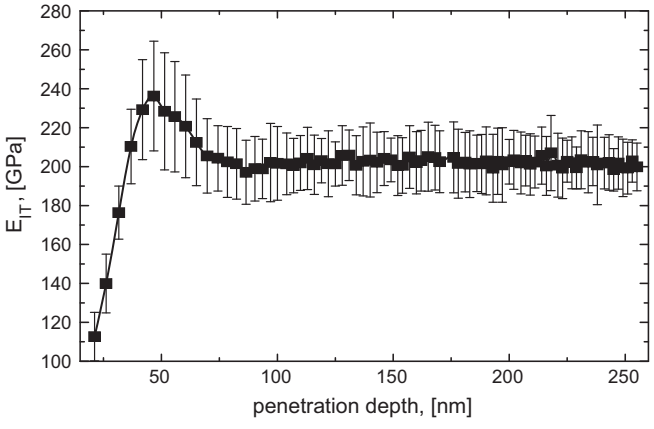

Fig. 2. Depth profile of the indentation modulus, E_{IT}, in the studied WC–C coatings.

Table 1
Summary of the surface properties of steel substrates with different surface finish and corresponding WC–C coatings obtained by contact profilometry and AFM.

Steel substrates	Surface finish	1 μm diamond	1 μm diamond	15 μm diamond	80/63 diamond disc	#80 SiC paper	As-ground	As-ground
Profilometry	R_a (nm)	24 ± 10	24 ± 7	135 ± 18	412 ± 40	450 ± 190	502 ± 30	573 ± 65
	R_z (nm)	176 ± 45	251 ± 51	1220 ± 140	3547 ± 350	3980 ± 165	3148 ± 900	3813 ± 230
	R_q (nm)	31 ± 16	31 ± 9	177 ± 26	545 ± 50	657 ± 320	631 ± 36	718 ± 86
AFM	R_a (nm)	3.0 ± 0.5	3.9 ± 2.2	105 ± 49	196 ± 85	303 ± 54	146 ± 46	139 ± 40
	R_z (nm)	14.4 ± 7.1	16.1 ± 7.9	181 ± 87	586 ± 372	117 ± 29	192 ± 28	212 ± 120
	R_q (nm)	5.3 ± 1	6.3 ± 3.7	136 ± 64	254 ± 110	41 ± 14	181 ± 54	166 ± 47
	R_{sk} (nm)	5.0 ± 1.2	3.5. ± 1.9	0.06 ± 0.4	−0.29 ± 0.5	−0.29 ± 0.6	0.06 ± 0.4	−0.18 ± 0.3
WC–C coating								
Profilometry	R_a (nm)	98 ± 168	99 ± 52	522 ± 77	662 ± 78	175 ± 58	555 ± 35	623 ± 24
	R_z (nm)	1177 ± 1374	1903 ± 1107	8663 ± 1148	7410 ± 902	2058 ± 55	4915 ± 566	5979 ± 646
	R_q (nm)	145 ± 213	158 ± 98	806 ± 89	865 ± 99	241 ± 95	698 ± 44	811 ± 42
AFM	R_a (nm)	25 ± 46	15.9 ± 4.4	81.8 ± 27.6	180 ± 47	34.4 ± 8.3	144 ± 62	138 ± 64
	R_z (nm)	521 ± 177	655 ± 368	189 ± 72	1181 ± 744	105 ± 36	449 ± 203	760 ± 779
	R_q (nm)	18.3 ± 4.2	22.3 ± 5.0	105.7 ± 35.5	222 ± 56	48.5 ± 12.1	178 ± 77	167 ± 75
	R_{sk} (nm)	3.7 ± 2.2	1.8 ± 0.9	0.20 ± 0.75	−0.29 ± 0.4	1.36 ± 0.86	0.10 ± 0.35	−0.04 ± 0.43

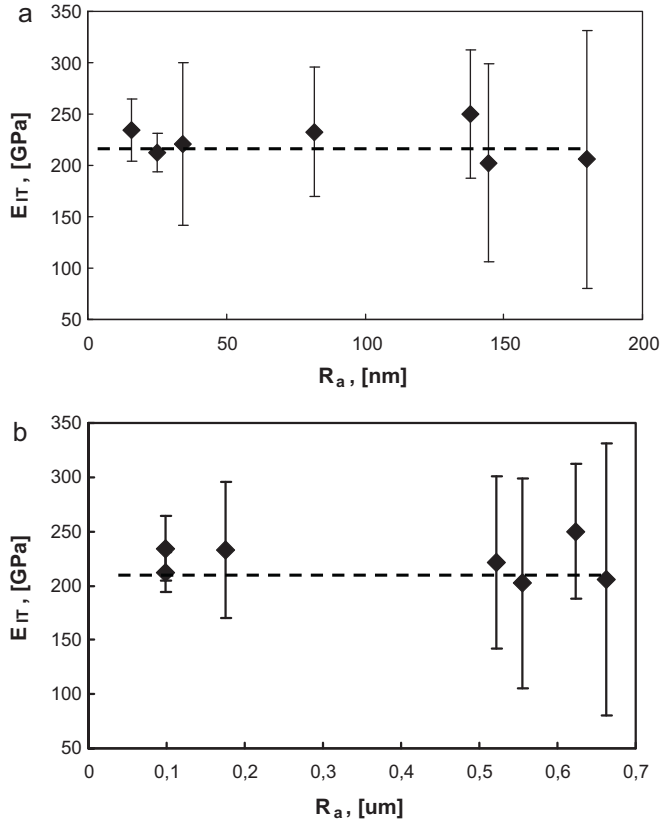

Fig. 3. The dependencies of the indentation modulus, E_{IT} on coating roughness determined from (a) microscopic area using AFM and (b) from macroscopic area using contact profilometry.

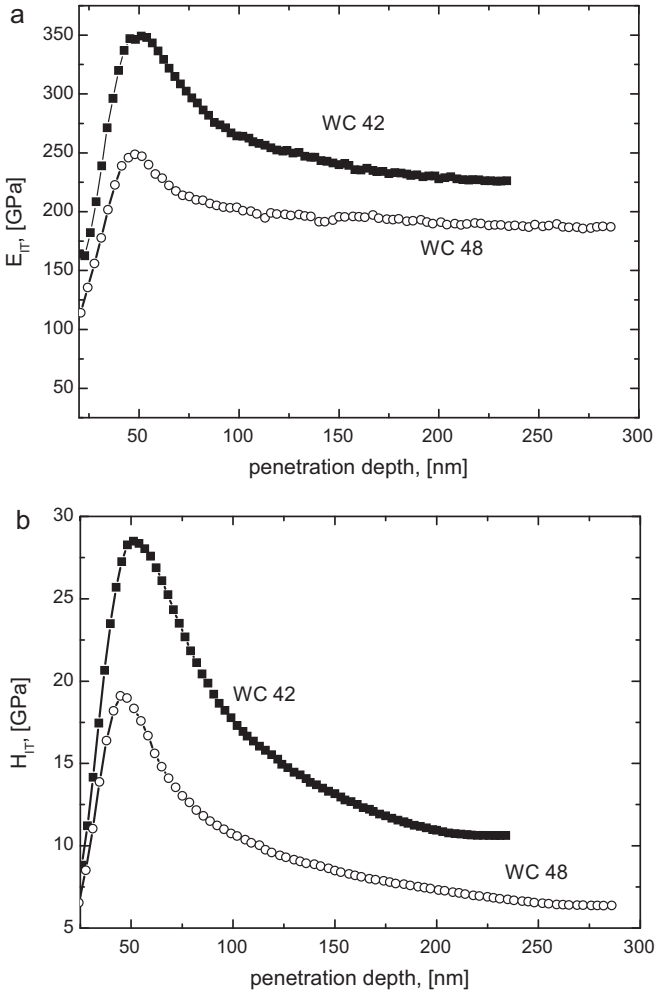

Fig. 4. The increase of the indentation modulus (a) and that of nanohardness (b) due to the optimization of the deposition conditions.

corresponding hardness is around 15.8 ± 2.5 GPa.[25] Because the lateral size of the indent and the depth of penetration are considerably larger than the size of the WC nanoparticles (around 10 nm), material can be considered as homogeneous at this scale and the above values as representatiove for the everage properties of the coating.

Fig. 3a and b shows the variations of E_{IT} of WC–C coating as a function of average R_a from AFM and contact profilometry, respectively. Despite some deviations, the values of indentation modulus oscillate within the studied R_a range at around 210–220 GPa regardless of the surface roughness and measurement method. The scatter in the range 9–14% both in indentation modulus and hardness at $R_a < 30$ nm increases up to 27–52% on the surfaces with higher roughness levels.[25] Thus, the accuracy of nanoindentation measurements of around 10–15% can be expected in case of WC–C coatings deposited on the well-polished substrates.

The nanoindentation measurements on such coatings revealed that the modification of the deposition conditions has strong effect on the resulting properties of WC–C coatings. The possibilities for the improvement of mechanical properties are clearly demonstrated in Fig. 4. Under the optimized deposition conditions, indentation modulus reached 350 GPa and the hardness over 28 GPa, which corresponds to more than 40% increase (compared to the standard case in Fig. 2). It is well above measurement uncertainty of 10%. The details of the optimization process were described earlier.[23,26]

3.3. Elastic modulus mapping

The results of quantitative nanomechanical measurements based on force–distance curves (PF QNM) recorded during soft (only elastic deformation under the tip occurs) tapping of the surface, are demonstrated in Fig. 5. Surface topography image in Fig. 5a is compared with the image of the elastic moduli in the studied nanocomposite WC–C coating in Fig. 5b. Color contrast enhanced by additional image treatment suggests the existence of at least two phases with different elastic moduli: dark (= softer) "grains" with the size up to 50–70 nm separated by a thin continuous net of a brighter (= stiffer) phase. The modulus contrast was only visible at relatively low imaging forces and vanished at higher loads. The comparison of both images implies that the net is independent of surface topography, therefore it seems to correspond to the amorphous carbon matrix phase and the islands to the clusters of WC nanocrystals. The determination of the absolute values of elastic moduli in different areas is not possible at this stage due to the absence of calibration.

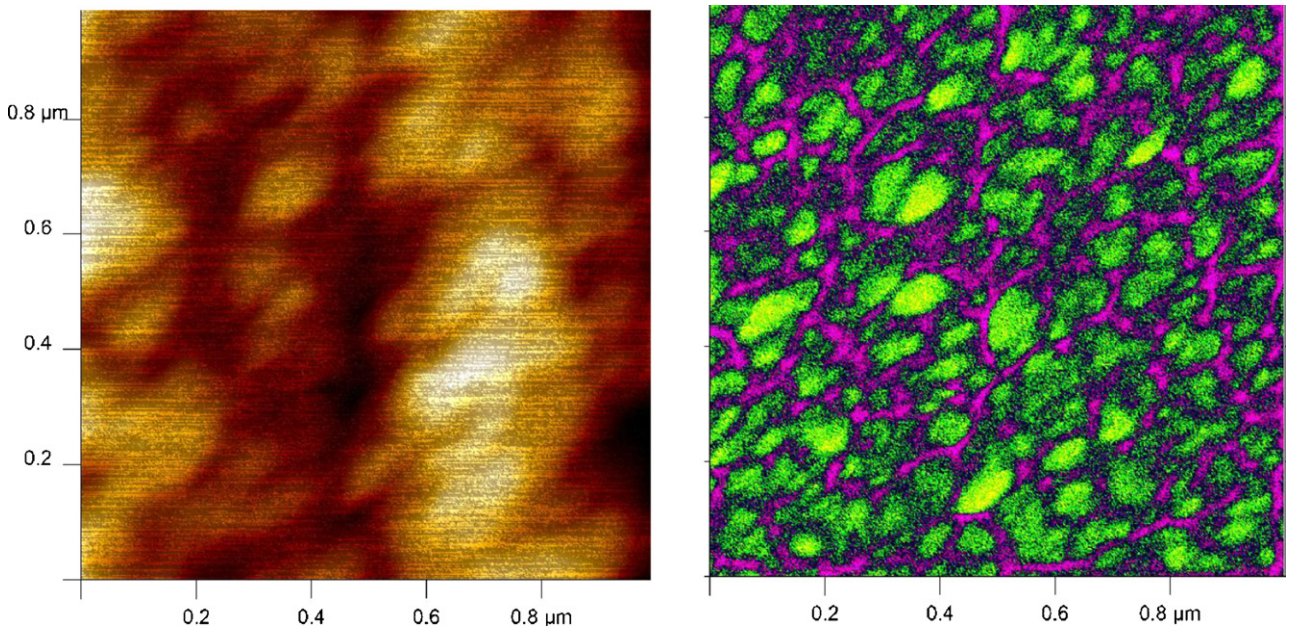

Fig. 5. PF QNM image of the surface topography of the nanocomposite WC–C coating (a) and of the corresponding relative elastic moduli (1 μm × 1 μm) distribution.

3.4. Friction

Fig. 6a shows the height image of WC–C coating deposited on 1 μm polished substrate and Fig. 6b and c illustrates the corresponding LFM images obtained during trace and retrace movement of the tip, respectively. The resulting LFM image without the effect of surface topography is obtained as a difference between trace and retrace friction images (Fig. 6d). Subtraction of the images doubles friction signal and eliminates the effect of misalignment of a photodetector and laser.[27]

The obtained LFM contrast is rather low and the visible features overlap with the topography of the surface. It suggests that the differences in COF among different areas are very weak and are related to surface morphology rather than to friction contrast. The exact determination of local COF was not possible up to now due to lack of proper calibration.

In contrary to only qualitative LFM images at nanolevel, Fig. 7 shows quantitative evolution of the coefficient of friction under load of 500 mN as a function of sliding distance at three different rates. The running-in stage is very short and after it, the values of COF stabilize within the range 0.11–0.17 almost regardless of sliding rate – the variations of COF are within the range of repeatability.

Following dependence (Fig. 8) illustrates analogous curves obtained in different samples under the same sliding rate. Most of the curves were below 0, although several samples exhibited steep increase of COF up to ~0.8 (not shown). The best coatings with reduced COF were around 0.11. Surface roughness had only very small and non-systematic influence on the measured COF behavior.

The difference among tribological behavior of WC–C at room and elevated temperatures is shown in Fig. 9. The increase of the operating temperature only to 100 °C caused increase of COF usually above 0.2 and up to 0.7–0.8 in the tests carried out at 450 °C. In contrast to room temperature behavior, significant scatter of the experimental data unrelated to surface topography was typical for elevated temperatures. Interestingly, the negligible effect of nitrogen atmosphere was found at 450 °C in comparison with the conventional behavior in air.[24,26]

4. Discussion

The investigation of the influence of surface roughness on elastic modulus and nanohardness of the studied PECVD nc-WC–C coatings shows that the correlation between R_a of the substrates and coatings is not linear.[25,28] The intrinsic roughness of the coatings on the well polished substrates ($R_a \sim 20$ nm) was in the range of around 100 nm regardless of the substrate roughness. When R_a of the substrates exceeded 100 nm, final roughness of the coatings was determined by the substrate roughness. The ISO standard requirement for the instrumented indentation at nano-loads is $R_a < 5\%$ of the indentation depth. In case of 10% penetration depth into 500 nm thin films it would mean $R_a < 3$ nm. This is not fulfilled even in very fine polished surfaces and results in the increase of experimental scatter. Fig. 3 confirms that the scatter of the elastic modulus is below 10–15% in the range of surface roughnesses determined by intrinsic topography of the coating compared to the topography controlled by the substrate roughness. Vice versa, scatter increased up to unacceptable 50% at higher roughness values, but because the number of measurements was sufficiently high, the average value remained the same regardless of the roughness.

The optimization of the deposition condition provides substantial increase of instrumented hardness and elastic modulus of PE CVD WC–C coatings even when the measurement uncertainty is taken into account (see Fig. 4). The contribution of nanostructure to hardness increase can be estimated in several ways. The easiest is a comparison with the literature data for the same coatings. Hardness of the commercially available

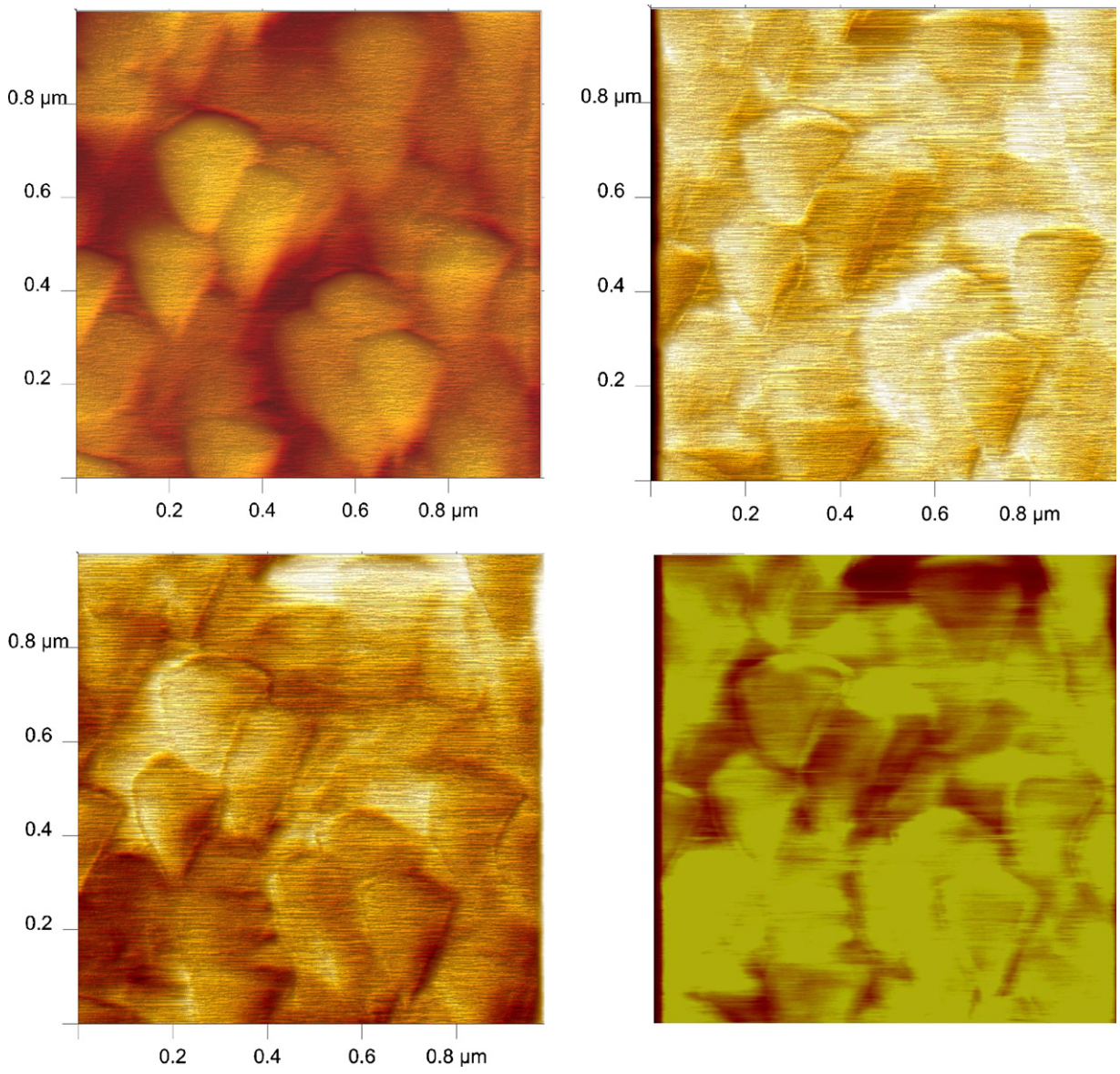

Fig. 6. LFM images of WC–C coating on steel substrate polished with 1 µm diamond slurry; (a) height image, (b) friction image during retrace movement of a tip, (c) "trace" image and (d) enhanced LFM image obtained as a difference between trace and retrace images.

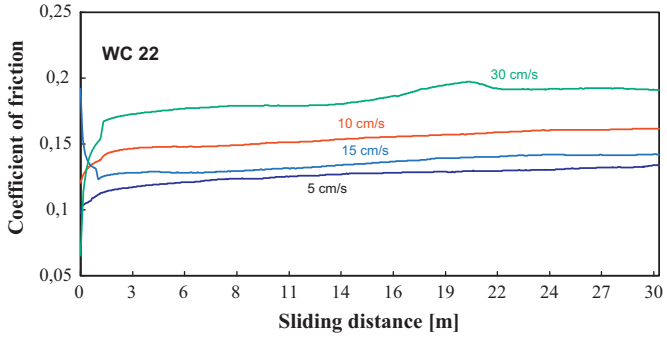

Fig. 7. A comparison of friction behavior in the studied WC–C coatings at different sliding rates.

WC–C coatings with lamellar structure is in the range HV 1000–2000 (~9.5–19 GPa),[29] which overlaps with the range of properties measured in the current unoptimized coatings. Nanocomposite structures resulting from optimization bring around 40% hardness increases. Assuming that the high hardness of the studied coatings originates solely from WC grains, another way is comparison with the maximum possible hardness of bulk polycrystalline WC. Our previous measurements on sintered bulk coarse-grained polycrystalline WC showed that its indentation modulus E_{IT} is 410 ± 37 GPa and hardness is 25.2 ± 2.9 GPa.[25,28] It is higher than in conventional WC–C coatings due to absence of softer carbon. If the same maximum values can be obtained in WC–C coatings with conventional structure, the excess in properties above that level would result from their nanocomposite structure. Simple estimation suggests that the nanocomposite effect is around 14%, which is close to the measurement error. The improvement is relatively small

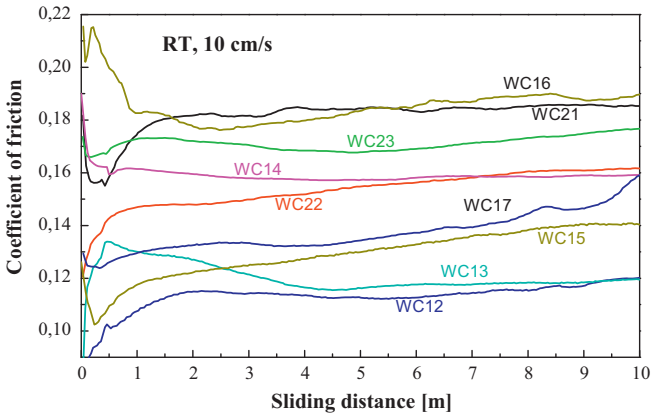

Fig. 8. Friction curves of various WC–C coatings deposited under different conditions as a function of sliding distance at sliding speed of 10 cm/s.

compared to the effect in the ultrahard ($H > 60$ GPa) nanocomposite TiN/a-Si_3N_4 coatings.[1] One more way to evaluate the role of nanostructure is the comparison with the properties of WC single crystals. They can be measured on individual grains in WC–Co sintered carbide and determined either from statistical distributions obtained from a large number of nanoindentation measurements or from nanoindents localized on individual WC grains. Statistical evaluation of hardness distributions from 300 indents in several WC–Co systems[30] allowed us to distinguish between harder (WC) and softer (Co) phase due to its bimodal character. Two peaks of indentation modulus distributions of WC grains were at around 430 GPa and 520 GPa and that of hardness at 29 GPa, while the peaks at around 340 GPa and 10 GPa, respectively, were attributed to binder phase.[30] This data cannot be used for the calculations not only because of the double peak of the elastic modulus of WC grains, but also because the distribution was very wide – the indentation modulus was in the range 400–700 GPa. Precisely localized nanoindentation measurements on individual grains confirmed the existence of wide scatter of E_{IT} and H_{IT}. Such scatter may be attributed to ISE, anisotropy of the elastic properties of WC grains ($H_{IT} > 40$ GPa for {1 0 1 0} and $H_{IT} = 25$–30 GPa for {0 0 0 1} orientation[31] as well as binder effect underneath of the WC grains. The obtained values in both cases are higher than those obtained in the optimized WC–C coatings containing much softer amorphous carbon phase. Thus, hardness optimization from the viewpoint of coating structure requires not only achieving WC nanocrystallites in carbon matrix, but also optimization of the ratio between the volume contents of hard and soft phases. Apparently, the possibilities to maximize stiffness and hardness of the studied WC–C coatings were not fully exploited yet.

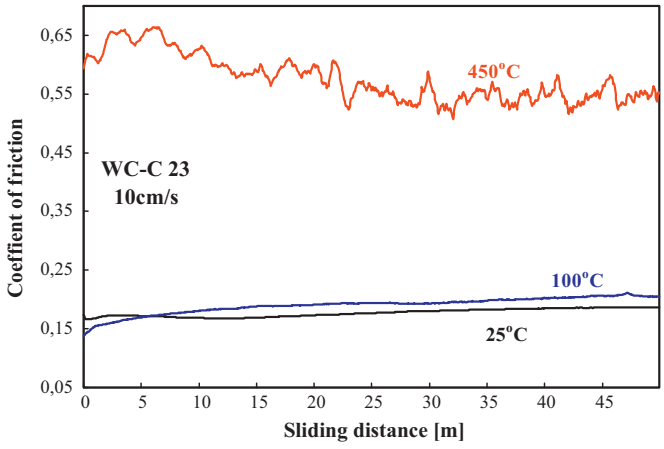

Fig. 9. The effect of temperature on friction behavior of WC–C coatings.

Fig. 5b shows a direct confirmation that PF QNM is able to visualize elastic properties of the materials with the stiffness well above 300 GPa with the lateral resolution close to nanoscale regardless of surface topography. This is a significant achievement because this mode was originally developed for bio- and polymeric materials with the stiffness below 100 GPa and so far it was not applied to such stiff materials. The condition for successful imaging of elastic properties is that special AFM cantilevers with high stiffness ($K = 2000$ N/m) and diamond tip are used to ensure that both AFM probe and tested material are elastically deformed during force tapping. Fully quantitative measurements using PF QNM require precise calibration and additional work on correct interpretation of the obtained images. Difficulty with the interpretation of the modulus image even at qualitative level is that nanoparticles may not be exposed on the surface and their location just under the surface may produce additional contrast without real physical meaning. This is also discussed later with the LFM images. Quantitative measurements are affected by the lack of precise reference values due to the wide range of elastic moduli of the individual WC grains mentioned earlier. The solution of this problem requires special study with PF QNM performed on the individual WC grains with their elastic modulus and hardness measured independently by nanoindentation.

The same conclusion concerning qualitative and quantitative data is valid for the application of AFM in the visualization of friction forces. The determination of the correlations among the macroscopic coefficient of friction and friction between two single asperities depends on the calibration of the individual tribo-pair "coating – AFM tip". The problem is that materials used for AFM tips (Si, Si_3N_4) are different from materials in real applications (steel, cemented carbide, etc.). Another difficulty which can explain the lack of friction contact in LFM image is that the scanned surface may be "homogeneous" – the whole surface is covered with a thin layer of carbon, adsorbed or reaction gases. They can overshadow the differences among individual phases in case of extremely low forces in LFM. On the other side, conventional tribological tests provide friction data from different tribo-pairs, macroscopic areas, considerably higher range of normal forces and therefore most probably, different wear mechanisms. The analysis of the correlations between LFM data even in case of its proper calibration and conventional ball-on-disc tests needs to consider all these factors.

The coefficients of friction with sufficient hardness are in the studied WC–C coatings in the range 0.1–0.2. The studies of the mechanisms operating during friction by Liu et al.[4] as well as our previous works[24,26] suggest the formation of a transfer film, which results in a low COF. This transfer film is mostly related to the oxidation of steel ball material in friction contacts at room

temperature tests and increased interactions between tungsten, iron and ambient air at elevated temperature tests.[4,24,26] Our future studies will be oriented on detailed investigations of the role of transfer films in friction and wear and mechanism of its formation at macro- and nano-scale. This work will include calibration and attempts of quantitative measurements using LFM and PF QNM modes on AFM.

5. Conclusion

The nanoindentation studies performed on the 500 nm thin nanocomposite PE CVD WC–C coatings with controlled roughness confirm that surface roughness substantially increases the scatter of the indentation modulus and hardness without affecting its average value. Surface roughness of the coatings below 30 nm is necessary to keep the scatter of indentation modulus and hardness below 15%. PF QNM mode in AFM was successfully applied for qualitative mapping of the elastic modulus of hard materials with the stiffness above 300 GPa. The condition was that special AFM cantilevers with high stiffness ($K = 2000$ N/m) and diamond tip were used. The studied WC–C coatings exhibited weak contrast in LFM and quantitative measurements, similarly as in the case of PF QNM, require precise calibration on individual WC grains with known properties. The studied WC–C coatings exhibit favorable room temperature friction behavior with the coefficients of friction below 0.2. The increase of temperature to 450 °C resulted in COF in the range 0.7–0.8 due to the interactions between tungsten, iron and ambient air and formation of a transfer film between the contacting surfaces. The optimization of the deposition conditions based on nanoindentation resulted in the increase of the indentation modulus from ∼220 GPa up to 350 GPa and that of the indentation hardness from ∼17 GPa to almost 29 GPa.

Acknowledgments

The contributions of P. Horňák with coating preparation, A. Duszová and G. Fuchsová with surface roughness and nanoindentation measurement, H. Stadler with PF QNM studies and P. Hvizdoš with data analysis are gratefully acknowledged. This work was supported by the following projects: APVV 0520-10, VEGA 2/0108/11 and MNT-ERA.NET HANCOC.

References

1. Vepřek S, Reprich S. A concept for the design of novel superhard coatings. *Thin Solid Films* 1995;**268**:64–71.
2. Hogmark S, Jacobson S, Larsson M. Design and evaluation of tribological coatings. *Wear* 2000;**246**:20–33.
3. Yang S, Camino D, Jones AHS, Teer DG. Deposition and tribological behaviour of sputtered carbon hard coatings. *Surf Coat Technol* 2000;**124**:110–6.
4. Liu Y, Gubisch M, Spiess L, Schaefer JA. Sliding friction of nanocomposite WC1−x/C coatings: transfer film and its influence on tribology. *J Nanosci Nanotechnol* 2009;**9**:3499–505.
5. Strondl C, Carvalho NM, De Hosson JThM, van der Kolk GJ. Investigation of the formation of tungsten carbide in tungsten-containing diamond like carbon coatings. *Surf Coat Technol* 2003;**162**:288–93.
6. Zeng XT, Zhang S, Ding X, Teer DG. Comparison of three types of carbon composite coatings with exceptional load-bearing capacity and high wear resistance. *Thin Solid Films* 2002;**420–421**:366–70.
7. Konca E, Cheng YT, Weiner AM, Dasch JM, Alpas A. Elevated temperature tribological behavior of non-hydrogenated diamond-like carbon coatings against 319 aluminum alloy. *Surf Coat Technol* 2006;**200**:3996–4005.
8. Lofaj F, Němeček J, Bláhová O. A comparative study of nanoindentation measurements on thin coatings. *Chemické Listy S* 2010;**109**:271–4.
9. ISO 14577-4:2007. Metallic materials – Instrumented indentation test for hardness and material parameters. Part 4 Test method for metallic and non-metallic coatings.
10. Fischer-Cripps AC. *Nanoindentation*. 2nd ed. New York: Springer; 2004.
11. Bull SJ, Page TF, Yoffe EH. An explanation of the indentation size effects in ceramics. *Philos Mag Lett* 1989;**59**:281–8.
12. Nix WD, Gao H. Indentation size effects in crystalline materials: a law for strain gradient plasticity. *J Mech Phys Solids* 1998;**46**:411–25.
13. Huang Y, Zhang F, Hwang KC, Nix WD, Pharr GM, Feng G. A model of size effects in nano-indentation. *J Mech Phys Solids* 2006;**54**:1668–86.
14. Taljat A, Pharr GM. Measurement of residual stresses by load and depth sensing spherical indentation. *Mater Res Soc Symp Proc* 2000;**594**:519–24.
15. Lee YH, Kwon D. Residual stresses in DLC/Si and Au/Si systems: application of a stress–relaxation model to nanoindentation technique. *J Mater Res* 2002;**17**:901–6.
16. Jiang WG, Su JJ, Feng XQ. Effect of surface roughness on nanoindentation test of thin films. *Eng Fracture Mech* 2008;**75**:4965–72.
17. Bouzakis KD, Michailidis N, Hadjiyiannis S, Skordaris G, Erkens G. The effect of specimen roughness and indenter tip geometry on the determination accuracy of thin hard coatings stress–strain laws by nanoindentation. *Mater Charact* 2003;**49**:149–56.
18. Mate CM, McClelland GM, Erlandsson R, Chiang S. Atomic scale friction of a Tungsten tip on a Graphite surface. *Phys Rev Lett* 1987;**59**:1942–5.
19. Meyer G, Amer NM. Simultaneous measurement of lateral and normal forces with an optical-beam-deflection atomic force microscope. *Appl Phys Lett* 1990;**57**:2089–91.
20. Hipp M, Bielefeldt H, Colchero J, Marti O, Mlynek J. A stand-alone scanning force and friction microscope. *Ultramicroscopy* 1992;**42–44**:1498–503.
21. Bhushan B. Introduction – measurement techniques and applications. In: Bhushan B, editor. *Handbook of micro/nanotribology*. Boca Ratom: CRC Press; 1999. p. 3–80.
22. http://www.bruker-axs.de/uploads/tx_linkselectorforpdfpool/PeakForce_Quantitative_Nanomechanical_Property_Mapping_brochure.pdf.
23. Kottfer D, Olejník F, Pešek L, Mrva P. Optimization of thin films deposition process. *Acta Met Slovaca* 2004;**10**:625–9.
24. Lofaj F, Hviščová P, Duszová A. Friction contact with the transfer films in the nanocomposite WC–C coatings. *Acta Met Slovaca* 2010;**16**:631–5.
25. Fuchsová G, Lofaj F, Simkulet V. The effect of surface roughness in nanoindentation. *Chemické Listy S* 2011;**105**:796–7.
26. Lofaj F, Mikula M, Grančič B, Cempura G, Horňák P, Kúš P, et al. Tribological properties of TiBx and WC/C coatings. *Ceramics–Silikáty* 2011;**55**:305–11.
27. Ruan J, Bhushan B. Atomic scale friction measurements using friction force microscopy. Part I – General principles and new measurement technique. *ASME J Tribol* 1994;**116**:378–88.
28. Lofaj F, Stadler H, Fuchsová G, Hvizdoš P, Duszová A. Elastic properties of thin WC/C coatings. *Chemické Listy S* 2011;**105**:684–7.
29. http://www.oerlikon.copm/balzers/.
30. Duszová A, Horňák P, Stoyka V, Hvizdoš P, Lofaj F, Dusza J. Microstructure parameters vs. load size effect in WC–Co hardmetals. *Chemické Listy S* 2011;**105**:792–3.
31. Bonache V, Rayón E, Salvador MD, Busquets D. Nanoindentation study of WC–12Co hardmetals obtained from nanocrystalline powders: evaluation of hardness and modulus on individual phases. *Mater Sci Eng A* 2010;**527**:2935–41.